# Insertion of methylene groups into functional molecules for high thermal stability and superior functionality of single-molecule transistors: a first-principles study

Furushima, Miku ; Uemoto, Mitsuharu ; Yin, Dongbao ; Izawa, Seiichiro ; Shintani, Ryo ; Majima, Yutaka ; Ono, Tomoya

(Citation)
New Journal of Chemistry,48(36):16008-16014

(Issue Date)
2024-08-20

(Resource Type)
journal article

(Version)
Accepted Manuscript

NJC
New Journal of Chemistry
A journal for new directions in chemistry

# Accepted Manuscript

This article can be cited before page numbers have been issued, to do this please use: M. Furushima, M. Uemoto, D. Yin, S. Izawa, R. Shintani, Y. Majima and T. Ono, *New J. Chem.*, 2024, DOI: 10.1039/D4NJ02610A.

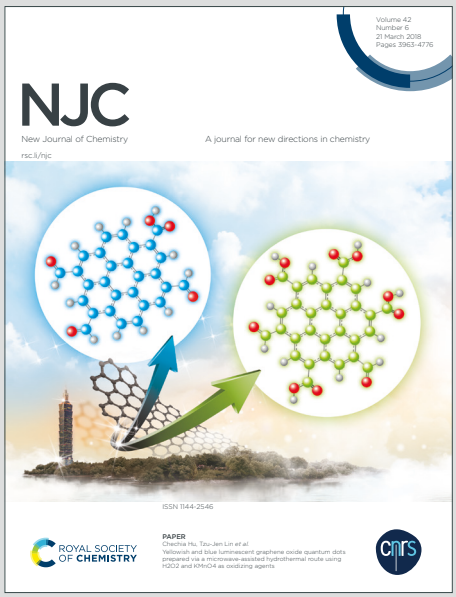

View Article Online
DOI: 10.1039/D4NJ02610A

Journal Name

ARTICLE TYPE

Cite this: DOI: 00.0000/xxxxxxxxxx

# Insertion of methylene groups to functional molecule for high thermal stability and superior functionality of single-molecule transistors: first-principles study†

Miku Furushima,*[a] Mitsuharu Uemoto,[a] Dongbao Yin,[b] Seiichiro Izawa,[b] Ryo Shintani,[c] Yutaka Majima,[b] and Tomoya Ono[a]

Received Date
Accepted Date

DOI: 00.0000/xxxxxxxxxx

The $\pi$-conjugated rigid molecule Bph is a candidate for use as a channel system of single-molecule transistors. In this first-principles study, the practicality of the chemical modification of the channel molecule Bph for enhancing stability and improving performance is discussed. The insertion of methylene groups into the edges of a channel is suggested to enhance the stability of the cross-linking structures between electrodes because of the relaxation of S bonds. The calculation of electronic states and transmission indicates the sufficient on current of the methylene-inserted Bph derivative (Bph–$CH_2$) in transistors through resonant tunneling. These results suggest the practicability for high stability and large on currents of inserting methylene groups as a method of modifying channel molecules to realize single-molecule transistors.

## 1 Introduction

One of the strategies to realize high-speed operation, high-degree integration, and low energy consumption for electronic computing systems is to develop smaller devices[1]. This strategy, which has the ultimate goal of realizing transistors with a single molecule, is attracting growing interest these days[2–4]. Single-molecule transistors, as the term implies, are transistors in which a single molecule is used as a channel to cross-link the source and drain electrodes, and the channel current is controlled by the gate electrodes nearby.

There are several methods of fabricating single-molecule junctions, such as the mechanically controllable break junction method[5], electromigration[6], and the scanning tunneling microscopy break junction method[7,8]. However, for practical applications, many electrodes with nanoscale gaps should be fabricated simultaneously and these methods, in which human efforts should be put into an every single junction one by one, are unsuitable. Recently, Majima's group has developed a suitable technique by combining lithography[9] and electroless Au plating (ELGP)[10,11]. In this method, electrode nanogaps have been fabricated simultaneously with 17-Å-scale precision since 2012[11], and channel molecules are expected to cross-link the electrodes.

One of the candidates for cross-linking channel molecules is a $\pi$-conjugated highly fused oligosilole derivative with two biphenyl groups (Bph; shown in Fig. 1a)[12] mainly for the following reasons:

- its conductivity originating from the rigid $\pi$-conjugated system[13,14],
- the spontaneous strong bonding of S atoms on both sides of the Bph molecule to Au electrodes[15],
- the stability of the backbone structure derived from Si atoms,
- the possible effect of lowering Fermi level pinning[16,17] by biphenyl groups, and
- the matching of the molecule length and the electrode nanogap, which possibly results in a self-assembled cross-linking structure.

The present method developed by Lee et al.[18] and Yin et al.[19] achieved several improvements, but the yield of the two-side-bonded structure is not sufficient. That is, it is important to realize a high thermal stability of the structure in which thiol groups on both sides of the molecule bond to the electrodes.

To increase the stability, the strict matching of the molecule length and the nanogap, which is a challenging undertaking in the ELGP method, is required. Therefore, another method of flexibly adjusting the molecule length, especially that providing flexibility for the molecule length with a spontaneous matching system

[a] Department of Electrical and Electronic Engineering, Graduate School of Engineering, Kobe University, Kobe, Hyogo 657-8501, Japan. Tel: +81-78-803-6497; E-mail: furushima@eedept.kobe-u.ac.jp
[b] Laboratory for Materials and Structures, Institute of Innovative Research, Tokyo Institute of Technology, Yokohama, Kanagawa 226-8503, Japan.
[c] Division of Chemistry, Department of Materials Engineering Science, Graduate School of Engineering Science, Osaka University, Toyonaka, Osaka 560-8531, Japan.
† Electronic Supplementary Information (ESI) available: See DOI: 00.0000/00000000.

View Article Online
DOI: 10.1039/D4NJ02610A

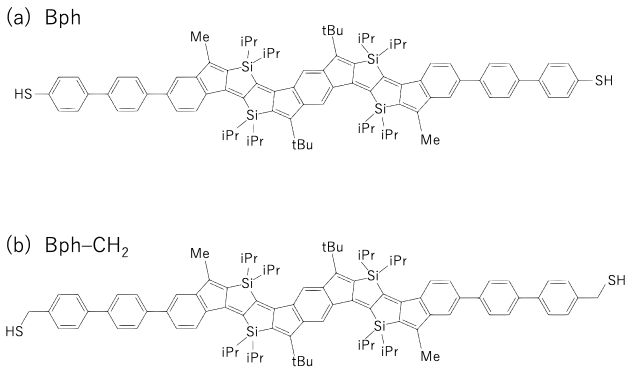


Fig. 1 Chemical structural formula of $\pi$-conjugated highly fused oligosilole derivatives in this work. (a) Molecule named Bph. (b) Modified molecule, noted as Bph–$CH_2$. "Me", "iPr", and "tBu" indicate methyl, *iso*-propyl, and *tert*-butyl groups, respectively.

is required. In this paper, on the basis of first-principles calculation, a method providing flexibility for the molecule length by inserting methylene groups between edge thiols and biphenyls is suggested and discussed, as illustrated in Fig. 1b. A single $\sigma$ bond is easy to rotate and thus has a high degree of freedom of rotation. On the other hand, the extent of the increase in stability and the change in the performance of a transistor are unknown. In this study, first, the stability of both-side-bonded structures are discussed with respect to the energy stability of the Bph molecule and the methylene-inserted Bph molecule (Bph–$CH_2$ molecule). Second, electronic states are determined by density functional theory (DFT) calculation[20]. Then, the local density of states (LDOS) and the ballistic electronic transmission[21] are obtained. From the results, the applicability of inserting methylene groups is confirmed where both higher stability and sufficient on currents are revealed.

## 2 Method

The structures and total energies of Bph and Bph–$CH_2$ molecules in vacuum and between two Au(111) electrodes with a gap length of 47.66 Å are obtained. The supercell sizes are $14.71 \times 16.98 \times 65.00$ Å$^3$ and $14.71 \times 16.98 \times 53.92$ Å$^3$ when in vacuum and between two electrodes, respectively. The obtained atomic geometries between two electrodes are shown in Fig. 2. During ionic relaxation, the positions of all Au ions and cell shapes are fixed. The binding energy $E_B$ of the molecules and electrodes is defined as

$$E_B = 3 \times E_{ele} + E_{mol} - E_{link} - 2 \times E_{H/ele}, \quad (1)$$

where $E_{ele}$, $E_{mol}$, $E_{link}$, and $E_{H/ele}$ are the total energies of electrodes, molecules, the cross-linking system, and a system of a H atom adsorbed on an electrode, respectively. DFT calculations[20] are carried out using the Vienna *ab initio* Simulation Package[22]. The pseudopotential generated by the projector augmented wave method[23] is used to describe electron–ion interactions. The Perdew–Burke–Ernzerhof functional within the general gradient approximation is employed[24]. The plane-wave basis set is used with a cutoff energy of 500 eV. Γ-centered $2\times2\times1$ $k$-point sampling is performed for $x$-, $y$-, and $z$-directions, where $z$ is the direction of the channel current. Ionic relaxation is performed until the norms of all the forces on the ions except Au become lower than 0.05 eV/Å.

The LDOSs of the channel molecules between the electrode shown in Fig. 2 are calculated under the following conditions using the RSPACE code[25,26], which employs the real-space finite-difference method[27] in the framework of DFT. The periodic boundary conditions are imposed on all directions of the supercell. The electron–ion interactions are described using norm-conserving pseudopotentials[28] of Troullier and Martins[29]. The exchange-correlation interaction is treated with in the local density approximation (LDA)[30]. Integration over the Brillouin zone is carried out using the Γ point. The supercell size is the same as the ionic relaxation condition for the molecules between two electrodes and the grid spacing in real space is taken to be $0.20 \times 0.18 \times 0.19$ Å$^3$. The self-consistent field calculation is continued until the change of the total energy becomes lower than $2.72\times10^{-5}$ eV, the common value as a threshold. Note that we confirmed that this grid spacing is fine enough for the electronic states to converge. The LDOS along the $z$-axis (the long axis of the molecules) is visualized. The LDOS is defined as

$$\rho(E,z) = \sum_i N e^{-\alpha(E-\varepsilon_i)^2} \iint |\Psi_i(x,y,z)|^2 dxdy, \quad (2)$$

where $E$ is the energy level, $x$, $y$, and $z$ are the cartesian coordinates, $\Psi_i$ and $\varepsilon_i$ are respectively the wavefunction and its eigenvalue of the $i$-th eigenstate, $\alpha$ is the smearing factor set to 135.1 eV$^{-2}$, and $N$ is the normalization factor ($= 2\sqrt{\alpha/\pi}$).

On the basis of the calculated electronic structure mentioned above, the electron transport properties of the molecule junction are investigated. The overbridging boundary-matching method[25,31,32] in the framework of DFT is adopted for transport property calculations. The models for such calculations are shown in Fig. 2, where the scattering region, which corresponds to the supercell to obtain the LDOS, is connected to the left (right) electrode on the left (right) side. The $k$-point mesh, the grid spacing, and the lateral length of the supercell in the electrode regions are chosen to correspond to those in the scattering region. Using the Kohn–Sham effective potential obtained under the periodic boundary condition, we computed the properties of the transport of the incident electrons originating from the left electrode under the semi-infinite boundary condition non-self-consistently[33] with energy values ranging from $-0.8$ eV to 2.0 eV in increments of 0.05 eV. It has been reported that this procedure is as accurate as that in the linear response regime but significantly more efficient than performing computations self-consistently on a scattering-wave basis. The transmission spectra are plotted using the transmission coefficients and group velocities obtained by the overbridging boundary-matching method.

## 3 Results and discussion

When the molecules are placed between the electrodes, each S atom locates near a bridge site of the first layer of Au(111) with chemical bonding. Moreover, the molecule long axis is almost vertical to the surfaces of the electrodes. The $E_B$ values are $-1.46$ and $-0.41$ eV for Bph and Bph–$CH_2$ molecules, respectively. The main reason why the $E_B$ of the Bph–$CH_2$ molecule is 1.05 eV

View Article Online
DOI: 10.1039/D4NJ02610A



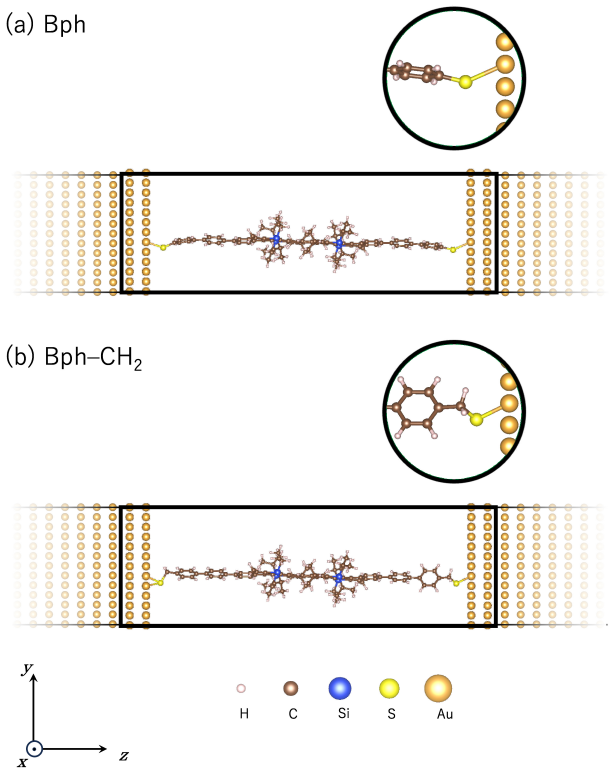


Fig. 2 Atomic geometries of Bph and Bph–$CH_2$ molecules between the electrodes. (a) Bph molecule. (b) Bph–$CH_2$ molecule. An enlarged view of surrounding S is exhibited in the circle on the upper right in each panel. The black thick straight lines are the boundaries of supercells. Note that the sticks between atoms do not always indicate chemical bonds but nearness.

higher than that of the Bph molecule is the distortion of the thiol groups in the anchor region, which form bonds to the electrodes. When a S atom locates at a bridge site, the natural angle of a S–C bond to the surface normal is about 60°, as revealed by a DFT study of the benzene thiolate bonding on Au(111)[34]. Therefore, the Bph molecule, which is rigid between S atoms at the both-side edges, cannot locate perpendicular to the surface without any distortion. Such an inevitable distortion can be found in the cross-linking structure in Fig. 2a. On the other hand, the Bph–$CH_2$ molecule, which has flexible methylene groups at the edges because of its easy rotation, can locate with the natural angle without any distortion. The structure in Fig. 2b also shows the chemical bonding with less distortion.

The twist of biphenyl groups is also affected by the distortion. The biphenyl twist angle $\theta$s, defined as the twist angle between the planes which include six C atoms of each benzene ring as shown in Fig. 3, are 27° (30°), and 40° (40°) for left-side (right-side) of Bph and left-side (right-side) of Bph–$CH_2$, respectively. The angle $\theta$ of the free biphenyl molecules in gas phase is 45°[35], which indicates that $\theta$ approaches the angle of free biphenyl molecules for Bph–$CH_2$ because of the less distortion and rotational degree of freedom derived from inserted methylene groups. The effect of twist angle $\theta$ on the electronic states and the transport property will be discussed later.

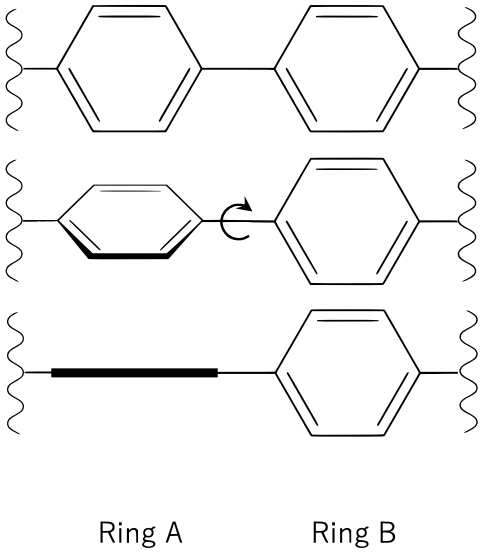


Fig. 3 Schematic image of the definition of the twist angle of the biphenyl groups $\theta$. The top, center, and bottom panels show the over views of the biphenyl groups with $\theta = 0°$, $0° < \theta < 90°$, $\theta = 90°$, respectively. The angle $\theta$ is defined as the twist angle of planes A and B, where planes A and B are the planes which include six C atoms of benzene rings A and B, respectively. When planes A and B are parallel or equivalent, $\theta = 0°$. Note that six C atoms of each benzene ring are not completely flat, therefore planes A and B are defined with use of least-square method where the sum of the square distance between the plane and each C atom is minimized.

For a qualitative discussion on transport properties, the LDOSs of Bph and Bph–$CH_2$ models are shown in Figs. 4a and c, respectively. For both molecules, the LDOS in the region where $|z| <$ 15 Å shows several horizontal bands corresponding to molecular orbitals (MOs), as is also shown in the contour curved lines in Figs. 4a and c. Such electronic states based on MOs can be clearly identified by converting the LDOS to one-dimensional profiles of density of states (DOS) of channel molecule regions. DOS of the channel molecule region ($|z| <$ 15 Å), defined as,

$$d(E) = \int_{z_{\min}}^{z_{\max}} \rho(E,z)dz, \qquad (3)$$

where $z_{\min} = -15$ Å and $z_{\max} = 15$ Å, are shown in Figs. 4b and d. These profiles exhibit several peaks originated from MOs. The levels of HOMO−1, HOMO, LUMO, and LUMO+1 of the isolated molecule calculated by the Becke three-parameter Lee–Yang–Parr functional[36–38] are shown in Table 1, where HOMO (LUMO) is the highest occupied (lowest unoccupied) MO and the notation −1 (+1) represents the next level below (above). Considering the trend of LDA, which underestimates the band gaps, MOs, LDOS, and DOS are consistent. These MO band structures are expected to contribute to the transmission of electrons via resonant tunneling[39], which will also be discussed later with the transport properties.

The ballistic transmittance of electrons in the range of $E = -0.8$ – 2.0 eV is calculated and shown in Figs. 4b and d. The transmittance spectrum of the Bph molecule shows two peaks above and two peaks below the Fermi level ($E_F$). The transmittance

View Article Online
DOI: 10.1039/D4NJ02610A



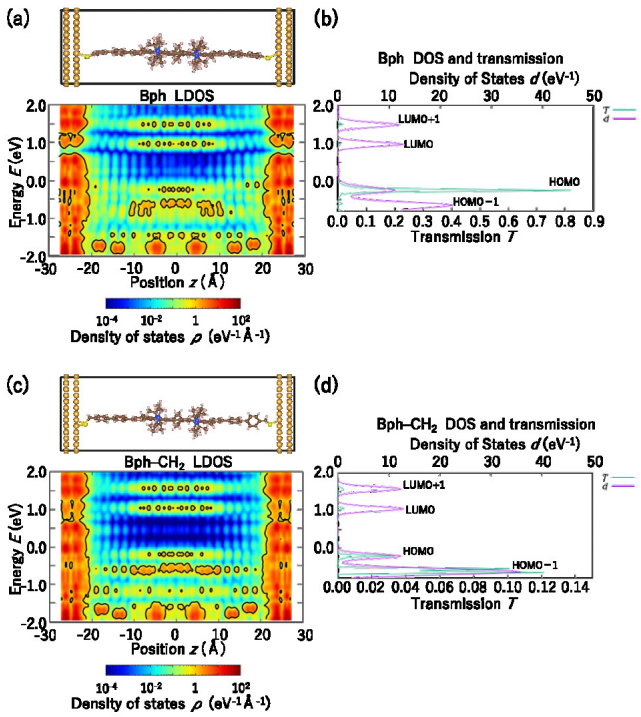


Fig. 4 LDOSs, DOSs, and transmission spectra. LDOSs of Bph and Bph–$CH_2$ models are shown in (a) and (c), respectively. Black contour curves, which correspond to $\rho = 0.65$ eV$^{-1}$Å$^{-1}$, are also shown on the maps to clearly identify the MO levels. For (a) and (c), the horizontal (vertical) axis shows the position $z$ (the energy level $E$). The Fermi level $E_F$ is equal to 0 eV. The density of states $d$ (purple curves) and the transmission spectra (green curves), as functions of energy, of Bph and Bph–$CH_2$ models are shown in (b) and (d), respectively. For comparing the LDOS and spatial position, the atomic geometries are exhibited above the LDOSs with the $z$ axes all the same. Moreover, for comparing the band levels of LDOS, DOS and transmission, the maps and spectra are placed with the heights of energy axes all the same. Considering the consistency of the MO levels and the transmission peaks, four of the peaks are attributed to HOMO−1, HOMO, LUMO and LUMO+1 as shown on the right side of the peaks. Note that linear interpolation is applied for spectra (b) and (d).

Table 1 MO levels in units of eV. MOs of an isolated molecule are calculated without periodic boundary conditions.

| Molecule | Bph | Bph–$CH_2$ |
|---|---|---|
| LUMO+1 | −1.90 | −1.93 |
| LUMO | −2.53 | −2.53 |
| HOMO | −4.76 | −4.76 |
| HOMO−1 | −5.22 | −5.22 |

spectrum of the Bph–$CH_2$ molecule exhibits two peaks above and two peaks below $E_F$. The peaks below $E_F$ are dominant for both molecules considering the transmission. These peak structures are consistent with our experimental results (see also, section S1 in ESI.). A $\pi$-conjugated highly fused oligosilole molecule with terphenyl and phenyl groups (Tph–ph) and its methylene-inserted derivative (Tph–ph–$CH_2$), which resemble Bph and Bph–$CH_2$ respectively, show several transmission peaks and nontransmissive band gaps. This consistency suggests the reliabilities of both theoretical and experimental results.

The energy levels of the transmission peaks in Figs. 4b and d roughly correspond to the MOs shown in the backbone regions in LDOS in Figs. 4a and c and in DOS in Figs. 4b and d. This result suggests that MOs function as transport paths of resonant tunneling[39], as briefly mentioned above. Moreover, interpeak regions have almost zero transmission, especially for the Bph–$CH_2$ model. This may make it easy to control the channel current by applying gate biases.

The heights of the HOMO and HOMO−1 peaks of the Bph–$CH_2$ molecule are 4% and 700% of those of Bph molecule, respectively[40]. We find that the transmission of Bph–$CH_2$ can be increased and decreased. From the obtained spectra, the channel currents are estimated by the following equation.

$$I = I_0 \int_E^0 T(E')dE', \tag{4}$$

where $I_0$ is the constant of proportionality and $E = -0.8$ eV corresponding to the drain bias of −0.8 V. The channel current ratio of Bph–$CH_2$ to Bph, $I_{\mathrm{Bph-CH_2}}/I_{\mathrm{Bph}} = 0.20$ is sufficiently large though of insulating property of methylene groups.

The channel current estimated above is sufficient, but we would like to seek for higher value. For this purpose, the mechanism of the transmission peak heights change is analyzed and discussed. In this paper, we focus on the insulating methylene groups, the twist of biphenyl groups, and the electronic states of biphenylthiol and biphenylmethanethiol which are the moieties at the edges.

Methylene groups, more generally, alkyl groups were revealed to be insulatiing[41]. For Bph, $\pi$-conjugated system is thought to underly on the area of five- or six-membered rings sharing $\pi$-electrons and $\pi$-electron-like lone pair electrons of S atoms[42]. For Bph–$CH_2$, however, $\pi$-conjugated system lies on only the area between the two biphenyl groups. Inserted methylene groups may have lowering effects on transmissions.

The twist angle of biphenyl groups also can be the origin of the transmission lowering. Biphenyl groups, which have $\pi$-conjugated electronic structures, is most conductive when it is flat and quantitatively, conductivity is proportional to $\cos^2\theta$[43–45]. As mentioned above, because of the rotational freedom of inserted methylene groups, the angle $\theta$ of Bph–$CH_2$ approaches 45°, the value of an isolated biphenyl molecule, which has steric hindrance between H atoms. The relation of the trade-off of the increasing the stability and decreasing the conductivity by the rotational degree of freedom of methylene groups is suggested.

These two factors mentioned above cannot explain the increase of HOMO−1 transmission by methylene insertion. To under-

View Article Online
DOI: 10.1039/D4NJ02610A



Table 2 Fermi level $E_F$s and orbital energies with respect to $E_F$s of biphenylthiol and biphenylmethanethiol molecules, which are the moieties of Bph and Bph–$CH_2$, respectively, in units of eV.

| | biphenylthiol | biphenylmethanethiol |
|---|---|---|
| $E_F$ | −4.55 | −4.02 |
| HOMO | −1.07 | −1.58 |
| HOMO−1 | −1.50 | −1.99 |
| HOMO−2 | −2.11 | −2.68 |
| HOMO−3 | −2.12 | −2.71 |

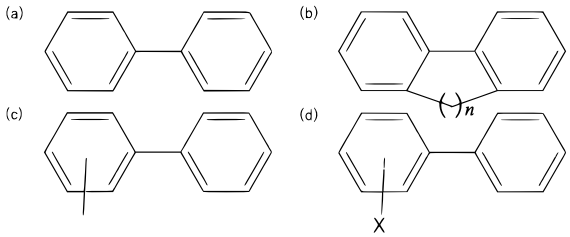


Fig. 5 Biphenyl molecule and chemical modification examples for biphenyl molecule. (a) Biphenyl molecule. (b) Alkyl-bridged molecule. (c) Molecule after methylation. (d) Molecule after halogenation. The character X indicates a halogen atom.

stand the origin of this, the relation between the changes of the electronic states and conductivities is discussed. Comparing the LDOSs in Fig. 4a and c, the regions of biphenyl groups ($|z|$ = 10–20 Å) exhibits difference. That is, for Bph, the energy level of the relatively high-$\rho$ area ($E = -0.5 - 0.0$ eV) is higher than HOMO−1 ($E = -0.60$ eV), while for Bph–$CH_2$, the level of relatively high-$\rho$ area is almost equal to HOMO−1 ($E = -0.60$ eV). To understand the origin of this difference, the orbital of the biphenylthiol and biphenylmethanethiol molecules are calculated and summarized in table 2 (See also the section S2 in ESI for computational details.). The latter biphenylmethanethiol molecule has 0.5 eV higher $E_F$ and thus the orbital energies with respect to $E_F$ are 0.5 eV lower comparing from the biphenylthiol molecule. These shifts, especially the shift of HOMO−1, are in agreement with the difference of LDOS. These facts suggest that methylene insertion increases the transmission of HOMO−1 via adjusting $E_F$ of biphenyl moiety.

We find the effect of insulating alkyl groups and furtherly, the two nontrivial effects on the transport property. One is the effect via the twist of biphenyl groups and the other is the effect via the orbital energy shift of edge moieties. These findings indicate that conductivity can be controlled by chemically modifying the biphenyl moieties. Examples of such chemical modifications include control of the twist angle by adding alkane bridge as shown in Fig. 5b and control of an orbital energies of edge moieties to match to that of backbone structure by introducing functional groups such as electron-donating methyl groups or an electron-withdrawing halogen as shown in Fig. 5c and d. The increases of the yields and conductivities upon these modifications is our futuristic topics.

## 4 Conclusion

We found that the Bph–$CH_2$ molecule with the both-side-bonded structure is more stable in energy than the Bph molecule and methylene groups insertion can be the method of designing a single-molecule transistor with sufficient on current. The binding energy of the Bph–$CH_2$ model is 1.05 eV larger than that of the Bph model, indicating the stability of the both-side-bonded structure. The origin of the difference in binding energy is the distortion of the bonding network around S atoms. The Bph–$CH_2$ model has the higher rotational degrees of freedom resulting in smaller distortions. The LDOSs show horizontal band structures, confirming that the transmission originates from resonant tunneling. The magnitudes of transmission can be larger or smaller depending on the MOs. The estimated on current of Bph–$CH_2$ is 20% that of Bph, indicating the sufficient on current of Bph–$CH_2$. The factors which change the peak heights in the transmission spectra are insulating methylene groups, twist angles of biphenyl groups affected by the molecule distortion, and $E_F$s of the edge moieties. These finding are guides for not only increasing the yield but also increasing the transmission.

## Conflicts of interest

There are no conflicts to declare.

## Acknowledgements

This work was partially financially supported by MEXT as part of the “Program for Promoting Researches on the Supercomputer Fugaku” (Quantum-Theory-Based Multiscale Simulations toward the Development of Next-Generation Energy-Saving Semiconductor Devices, JPMXP1020200205) and also supported as part of the JSPS KAKENHI (JP22H05463), JST CREST (JPMJCR22B4), and JSPS Core-to-Core Program (JPJSCCA20230005). The numerical calculations were carried out using the computer facilities of the Institute for Solid State Physics at The University of Tokyo and the supercomputer Fugaku provided by the RIKEN Center for Computational Science (Project ID: hp230175).

View Article Online
DOI: 10.1039/D4NJ02610A



## Notes and references


1 D. Xiang, X. Wang, C. Jia, T. Lee and X. Guo, *Chem. Rev.*, 2016, **116**, 4318–4440.

2 M. L. Perrin, E. Burzurí and H. S. J. van der Zant, *Chem. Soc. Rev.*, 2015, **44**, 902–919.

3 Y. Li, W. Xu, Y.-L. Zou, J. Li, T. Gao, R. Huang, L. Chen, Z. Xiao, J. Shi, Y. Yang and W. Hong, *Adv. Funct. Mater.*, 2023, **33**, 2302985.

4 Z. Chen, I. M. Grace, S. L. Woltering, L. Chen, A. Gee, J. Baugh, G. A. D. Briggs, L. Bogani, J. A. Mol, C. J. Lambert, H. L. Anderson and J. O. Thomas, *Nat. Nanotechnol.*, 2024.

5 M. A. Reed, C. Zhou, C. J. Muller, T. P. Burgin and J. M. Tour, *Science*, 1997, **278**, 252–254.

6 Y. Noguchi, T. Nagase, T. Kubota, T. Kamikado and S. Mashiko, *Thin Solid Films*, 2006, **499**, 90–94.

7 X.-S. Zhou, Y.-M. Wei, L. Liu, Z.-B. Chen, J. Tang and B.-W. Mao, *J. Am. Chem. Soc.*, 2008, **130**, 13228–13230.

8 X.-S. Zhou, J.-H. Liang, Z.-B. Chen and B.-W. Mao, *Electrochem. Commun.*, 2011, **13**, 407–410.

9 C. Vieu, F. Carcenac, A. Pépin, Y. Chen, M. M, A. Lebib, L. Manin-Ferlazzo, L. Couraud and H. Launois, *Appl. Surf. Sci.*, 2000, **164**, 111–117.

10 Y. Y. Choi, A. Kwon and Y. Majima, *Appl. Phys. Express*, 2019, **12**, 125003.

11 V. M. Serdio V., Y. Azuma, S. Takeshita, T. Muraki, T. Teranishi and Y. Majima, *Nanoscale*, 2012, **4**, 7161–7167.

12 N. Hamada, T. Tsuda and R. Shintani, *Eur. J. Org. Chem.*, 2021, **2021**, 4824–4827.

13 H. Tsuji and E. Nakamura, *Acc. Chem. Res.*, 2019, **52**, 2939–2949.

14 W. Chen, J. R. Widawsky, H. Vázquez, S. T. Schneebeli, M. S. Hybertsen, R. Breslow and L. Venkataraman, *J. Am. Chem. Soc.*, 2011, **133**, 17160–17163.

15 H. Häkkinen, *Nat. Chem.*, 2012, **4**, 443–455.

16 J. Jang, H.-S. Ra, J. Ahn, T. W. Kim, S. H. Song, S. Park, T. Taniguchi, K. Watanabe, K. Lee and D. K. Hwang, *Adv. Mater.*, 2022, **34**, 2109899.

17 G. Heimel, L. Romaner, J.-L. Brédas and E. Zojer, *Phys. Rev. Lett.*, 2006, **96**, 196806.

18 S. J. Lee, J. Kim, T. Tsuda, R. Takano, R. Shintani, K. Nozaki and Y. Majima, *Appl. Phys. Express*, 2019, **12**, 125007.

19 D. Yin, M. Furushima, E. Tsuchihata, S. Izawa, T. Ono, R. Shintani and Y. Majima, *Adv. Electron. Mater.*, 2400390.

20 P. Hohenberg and W. Kohn, *Phys. Rev.*, 1964, **136**, B864–B871.

21 K. M. Schep, P. J. Kelly and G. E. W. Bauer, *Phys. Rev. B*, 1998, **57**, 8907–8926.

22 G. Kresse and J. Furthmüller, *Phys. Rev. B*, 1996, **54**, 11169–11186.

23 P. E. Blöchl, *Phys. Rev. B*, 1994, **50**, 17953–17979.

24 J. P. Perdew, K. Burke and M. Ernzerhof, *Phys. Rev. Lett.*, 1996, **77**, 3865–3868.

25 K. Hirose, T. Ono, Y. Fujimoto and S. Tsukamoto, *First-principles calculations in real-space formalism: electronic configurations and transport properties of nanostructures*, World Scientific, 2005.

26 T. Ono, M. Heide, N. Atodiresei, P. Baumeister, S. Tsukamoto and S. Blügel, *Phys. Rev. B*, 2010, **82**, 205115.

27 J. R. Chelikowsky, N. Troullier and Y. Saad, *Phys. Rev. Lett.*, 1994, **72**, 1240–1243.

28 *We used the norm-conserving pseudopotentials NCPS97 constructed by K. Kobayashi. See K. Kobayashi, Comput. Mater. Sci.* **14**, *72 (1999)*.

29 N. Troullier and J. L. Martins, *Phys. Rev. B*, 1991, **43**, 1993–2006.

30 S. H. Vosko, L. Wilk and M. Nusair, *Can. J. Phys.*, 1980, **58**, 1200–1211.

31 Y. Fujimoto and K. Hirose, *Phys. Rev. B*, 2003, **67**, 195315.

32 T. Ono, Y. Egami and K. Hirose, *Phys. Rev. B*, 2012, **86**, 195406.

33 L. Kong, J. R. Chelikowsky, J. B. Neaton and S. G. Louie, *Phys. Rev. B*, 2007, **76**, 235422.

34 J. Nara, S. Higai, Y. Morikawa and T. Ohno, *J. Chem. Phys.*, 2004, **120**, 6705–6711.

35 F. Grein, *J. Phys. Chem. A*, 2002, **106**, 3823–3827.

36 A. D. Becke, *Phys. Rev. A*, 1988, **38**, 3098–3100.

37 C. Lee, W. Yang and R. G. Parr, *Phys. Rev. B*, 1988, **37**, 785–789.

38 *Becke three-parameter Lee–Yang–Parr functional with 6–31G(d) basis set was used to calculate MOs using the General Atomic and Molecular Electronic Structure System (GAMESS). For GAMESS, see G. M. J. Barca, C. Bertoni, L. Carrington, D. Datta, N. De Silva, J. E. Deustua, D. G. Fedorov, J. R. Gour, A. O. Gunina, E. Guidez, T. Harville, S. Irle, J. Ivanic, K. Kowalski, S. S. Leang, H. Li, W. Li, J. J. Lutz, I. Magoulas, J. Mato, V. Mironov, H. Nakata, B. Q. Pham, P. Piecuch, D. Poole, S. R. Pruitt, A. P. Rendell, L. B. Roskop, K. Ruedenberg, T. Sattasathuchana, M. W. Schmidt, J. Shen, L. Slipchenko, M. Sosonkina, V. Sundriyal, A. Tiwari, J. L. Galvez Vallejo, B. Westheimer, M. Włoch, P. Xu, F. Zahariev, M. S. Gordon, J. Chem. Phys.* **152**, *154102 (2020)*.

39 L. Britnell, R. V. Gorbachev, A. K. Geim, L. A. Ponomarenko, A. Mishchenko, M. T. Greenaway, T. M. Fromhold, K. S. Novoselov and L. Eaves, *Nat. Commun.*, 2013, **4**, 1794.

40 *The peak heights may depend on increment values of energy and interpolation methods. We have evaluated the accuracy of heights of transmission peaks by changing increment values of energy (0.05 eV or 0.1 eV) and interpolation method (linear interpolation or spline interpolation). The result is as follows. The ratio for HOMO ranges from 4% to 27%, the values less than 100%, and the ratio for HOMO−1 ranges from 267% to 714%, the values greater than 100%.*

41 H. Liu, N. Wang, J. Zhao, Y. Guo, X. Yin, F. Y. C. Boey and H. Zhang, *ChemPhysChem*, 2008, **9**, 1416–1424.

42 R.-W. Yan, X. Jin, S.-Y. Guan, X.-G. Zhang, R. Pang, Z.-Q. Tian, D.-Y. Wu and B.-W. Mao, *J. Phys. Chem. C*, 2016, **120**, 11820–11830.

43 L. Venkataraman, J. E. Klare, C. Nuckolls, M. S. Hybertsen

View Article Online
DOI: 10.1039/D4NJ02610A

and M. L. Steigerwald, *Nature*, 2006, **442**, 904–907.

44 A. Mishchenko, D. Vonlanthen, V. Meded, M. Bürkle, C. Li, I. V. Pobelov, A. Bagrets, J. K. Viljas, F. Pauly, F. Evers, M. Mayor and T. Wandlowski, *Nano Lett.*, 2010, **10**, 156–163.

45 M. E. Z. Michoff, M. E. Castillo and E. P. M. Leiva, *J. Phys. Chem. C*, 2013, **117**, 25724–25732.

View Article Online
DOI: 10.1039/D4NJ02610A

## Data availability statements

A part of the data was obtained from the RSPACE code, which is not available due to legal confidential requirements.